Neuron, Vol. 21, 1259–1272, December, 1998, Copyright ©1998 by Cell Press

Essential Roles for the Abl and Arg Tyrosine Kinases in Neurulation

Anthony J. Koleske,*‖#, Ann M. Gifford,* Martin L. Scott,* Michelle Nee,* Roderick T. Bronson,† Klaus A. Miczek,‡ and David Baltimore*§

*Department of Biology
Massachusetts Institute of Technology
Cambridge, Massachusetts 02139

†Department of Pathology
Tufts University Schools of Medicine and Veterinary Medicine
Boston, Massachusetts 02111

‡Department of Psychology, Pharmacology, and Psychiatry
Tufts University
Medford, Massachusetts 02155

§California Institute of Technology
Pasadena, California 91125

Summary

The Abl and Arg tyrosine kinases play fundamental roles in the development and function of the central nervous system. Arg is most abundant in adult mouse brain, especially in synapse-rich regions. *arg*$^{-/-}$ mice develop normally but exhibit multiple behavioral abnormalities, suggesting that *arg*$^{-/-}$ brains suffer from defects in neuronal function. Embryos deficient in both Abl and Arg suffer from defects in neurulation and die before 11 days postcoitum (dpc). Although they divide normally, *abl*$^{-/-}$*arg*$^{-/-}$ neuroepithelial cells display gross alterations in their actin cytoskeleton. We find that Abl and Arg colocalize with each other and with actin microfilaments at the apical surface of the developing neuroepithelium. Thus, Abl and Arg play essential roles in neurulation and can regulate the structure of the actin cytoskeleton.

Introduction

The Abl family of nonreceptor tyrosine kinases in vertebrates consists of Abl and Arg (the Abl-related gene) (Wang et al., 1984; Kruh et al., 1986). These proteins exhibit extensive conservation in sequence and architecture. Following a short N-terminal domain, each protein contains tandem SH3, SH2, and tyrosine kinase domains that share 89%, 90%, and 93% identity, respectively. The SH3 and SH2 domains regulate the kinase activity, both by interacting with the kinase domain and by binding targets and effectors of the kinase (see Mayer and Baltimore, 1994 and references therein). In both proteins, the first 135 amino acids following the kinase domain also contain three conserved PXXP motifs that can serve as binding sites for SH3 domains (Ren et al., 1994; Dai and Pendergast, 1995; Shi et al., 1995; Wang et al., 1996). Abl and Arg also share C-terminal globular (G-) and filamentous (F-) actin binding domains (Van Etten et al., 1994), which are not found in other nonreceptor tyrosine kinases. This conservation of structure suggests that Abl and Arg may regulate similar cellular functions.

Although the signaling pathways that employ these kinases are not well defined, mutational studies suggest that both Abl and Arg interact functionally with cellular growth regulatory pathways. Mutant forms of Abl or Arg can lead to the oncogenic transformation of cells, and mutations in *abl* cause leukemias in mammals (see Rosenberg and Witte, 1988; Daley and Ben-Neriah, 1991; Mayer and Baltimore, 1994; Mysliwiec et al., 1996; and references therein).

Genetic studies indicate that the Abl family kinases can regulate cellular morphology and motility through interactions with the actin cytoskeleton. In fly embryos, *Drosophila* (D)-Abl acts within developing neurons to regulate fasciculation and axonal outgrowth (Gertler et al., 1989, 1993). A haploinsufficiency in the *enabled* gene suppresses some of the *D-abl*-dependent phenotypes (Gertler et al., 1990). In cultured fibroblasts, the mammalian Enabled protein (Mena) localizes to focal contacts and lamellapodia, where it binds profilin and potentiates the outgrowth of actin-rich structures (Gertler et al., 1996). These data imply that the defects in neurogenesis of flies containing *D-abl* mutations result from faulty regulation of the actin cytoskeleton or misinterpretation of signals generated within this network.

Other experiments also point to functional interactions between Abl and the actin cytoskeleton. The clustering of integrins, which serve as docking sites for actin stress fibers, activates Abl kinase activity (Lewis et al., 1996). The Bcr-Abl and Tel-Abl oncoproteins both colocalize with actin stress fibers in vivo (McWhirter and Wang, 1991; Golub et al., 1996). In fact, Bcr-Abl can evoke multiple changes in the actin cytoskeleton, leading to increases in cellular motility, membrane ruffling, and filipodial extension (Salgia et al., 1997). Thus, Abl and Arg may integrate morphological and growth regulatory cues within the cell.

Previous studies have demonstrated critical roles for Abl in mouse development. Mice homozygous for an *abl* null mutation display pleiotropic developmental phenotypes (Schwartzberg et al., 1991; Tybulewicz et al., 1991). Some *abl*$^{-/-}$ mice that survive to adulthood are lymphopenic, having lower than normal central and peripheral levels of mature B and T cells. However, the penetrance of this phenotype is incomplete and does not depend on strain background (Hardin et al., 1995).

Both Abl and Arg are widely expressed in adult tissues. This observation and the high degree of identity shared between Abl and Arg suggest that these proteins serve similar functions in vivo. It is possible, for example, that Arg fully compensates for the Abl-deficiency in mice that are not lymphopenic. Arg and Abl may also play overlapping roles in the development or function of

‖To whom correspondence should be addressed (e-mail: anthony.koleske@yale.edu).

#Present address: Department of Molecular Biophysics and Biochemistry, Yale University, New Haven, Connecticut 06520.

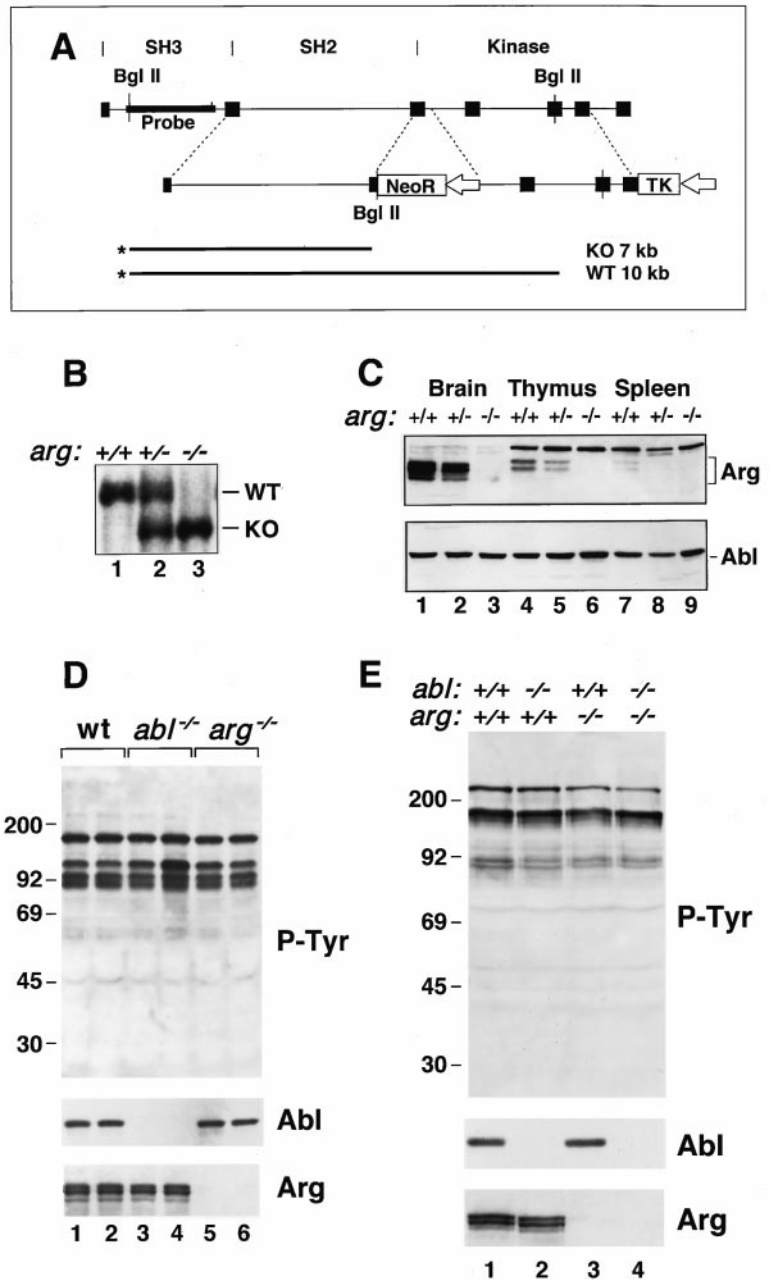

Figure 1. Generation of *arg*$^{-/-}$ Mice

(A) Targeting of the *arg* gene. A map of the targeting vector is shown. Exons (in gray) correspond to the domain structure shown above the figure. BglII restriction sites are also shown. Southern blot analysis of BglII-digested genomic DNA yielded a 10 kb signal for the wild-type locus and a 7 kb band for the targeted locus using the indicated probe (in black).

(B) Southern blot analysis of tail DNA from progeny of *arg*$^{+/-}$ intercrosses. Genotypes are indicated on the top. The wild-type (WT) and *arg* knockout (KO) bands are indicated.

(C) Western blot analysis of tissue extracts from *arg*$^{+/+}$, *arg*$^{+/-}$, and *arg*$^{-/-}$ mice. Protein (100 μg) from brain (lanes 1–3), thymus (lanes 4–6), and spleen (lanes 7–9) was separated on a 7.5% SDS-PAGE gel and blotted to a membrane. The *arg* genotypes of the mice are indicated at the top of the figure. The membrane was probed with antibodies to Arg or Abl. Abl appears as a discrete band of 145 kDa as indicated. Arg appears as a set of bands of 135–150 kDa as indicated. Brain Arg exhibits a 7–10 kDa increased mobility relative to Arg from spleen and thymus. A nonspecific band of 190 kDa crossreacts with the anti-Arg antibodies and serves as a loading control.

(D) Western blot analysis of wild-type, *abl*$^{-/-}$, and *arg*$^{-/-}$ extracts. Protein (100 μg) extracted from the cerebral cortex of two different wild-type (lanes 1 and 2), *abl*$^{-/-}$ (lanes 3 and 4), or *arg*$^{-/-}$ (lanes 5 and 6) mice was separated on a 10% SDS-PAGE gel and blotted to a membrane. The membrane was probed with antibodies to phosphotyrosine, Abl, and Arg. Molecular weight standards (in kDa) are shown to the left (top panel).

(E) Western blot analysis of 9.5 dpc embryo extracts. Protein (100 μg) extracted from wild-type (lane 1), *abl*$^{-/-}$ (lane 2), *arg*$^{-/-}$ (lane 3), or *abl*$^{-/-}$*arg*$^{-/-}$ (lane 4) embryos (9.5 dpc) was separated on a 10% SDS-PAGE gel and blotted to a membrane. The membranes were probed with antibodies to phosphotyrosine, Abl, or Arg. Molecular weight standards (in kDa) are shown to the left (top panel).

many other tissues. To identify the processes that depend on both Abl and Arg for proper execution, we studied the development of mice lacking both kinases.

We present evidence here that Arg and Abl play fundamental roles in the development and function of the central nervous system. We have utilized embryonic stem (ES) cell technology to inactivate the *arg* gene in mice. Analysis of *arg*$^{-/-}$ mice has revealed a previously unappreciated role for Arg in normal brain function. We have intercrossed *arg* and *abl* mutant mice to identify roles for these kinases in development. These studies have revealed that normal neurulation requires either Abl or Arg.

Results

Inactivation of the *arg* Gene

The DNA encoding amino acids 287(D) to 320(K) of *arg*, the N-terminal portion of the kinase domain, was replaced with a *neo*^{R} selectable marker in ES cells (Figure 1A). Chimeras made from these cells transmitted the *arg*$^{-}$ allele to offspring (Figure 1B). Western blot analysis (see below) demonstrated the total absence of Arg protein in tissue extracts from *arg*$^{-/-}$ animals (Figure 1C). All experiments presented in this paper were performed using mice of a mixed (129/SvJ × C57BL/6) genetic background.

Table 1. Progeny of $arg^{+/-}$ Intercrosses (n = 55)

arg	Expected (%)	Observed (%)
+/+	138 (25)	155 (28.1)
+/−	276 (50)	265 (48.1)
−/−	138 (25)	131 (23.8)

Mice were genotyped at 10–14 days post partum (dpp). The expected and observed frequencies (and percentages) of each genotype are presented (n = number of progeny analyzed).

Viability of $arg^{-/-}$ Mice

$arg^{-/-}$ mice were obtained from crosses of $arg^{+/-}$ mice at Mendelian ratios (Table 1). Histological analysis of $arg^{-/-}$ mice revealed no abnormalities. In addition, analysis of cells of the blood, spleen, bone marrow, and thymus indicated no hematopoietic abnormalities in $arg^{-/-}$ mice. $arg^{-/-}$ pups were runted, weighing 79.6% ± 3.6% of wild-type littermates at 3 weeks of age. At 8 weeks of age, however, $arg^{-/-}$ mice did not differ significantly in weight from littermates (100% ± 4.2% of littermate controls).

Expression of Abl and Arg in $abl^{-/-}$ and $arg^{-/-}$ Mice

Compared with other adult tissues, whole brain extracts contained the highest levels of Arg protein (Figure 1C). Significant levels of Arg were also detected in spleen and thymus extracts, while other tissues showed lower levels of Arg (Figure 1C and data not shown). Identical results were obtained with antibodies that recognized N-terminal, central, or C-terminal portions of Arg (data not shown). The mobility of Arg in brain extracts was 9–10 kDa faster than the spleen or thymus isoforms. This was due to the specific exclusion of an exon encoding amino acids 688(G) to 791(S) in the brain (A. J. K. and D. B., unpublished data).

In tissues from adult mice, Abl levels were not elevated in $arg^{-/-}$ mice as compared with wild-type or $arg^{+/-}$ mice (Figure 1C, lanes 3, 6, and 9). Similarly, wild-type levels of Arg were observed in extracts from $abl^{-/-}$ cerebral cortex (Figure 1D, lanes 3 and 4) and other tissues (data not shown). We did not detect any alterations in the patterns of the major phosphotyrosine-containing proteins in cortical extracts from $abl^{-/-}$ and $arg^{-/-}$ mice (Figure 1D). Similarly, no significant differences in the major phosphotyrosine-containing proteins were observed in extracts from the cerebellum, spleen, or thymus from wild-type, $abl^{-/-}$, or $arg^{-/-}$ mice (data not shown).

Localization of Arg within the Brain

We localized Arg in the brain by immunohistochemistry. Arg was concentrated in regions of the brain enriched in synapses and was nearly absent in cell body–rich regions of the brain (Figure 2). For example, Arg was very abundant in the molecular layer of the cerebellum, where the axons of parallel fibers and climbing fibers form synaptic connections with Purkinje cells (Figure 2D). Much less Arg was found in the granular layer of the cerebellum, which is tightly packed with the cell bodies of granular neurons, and Arg was absent from

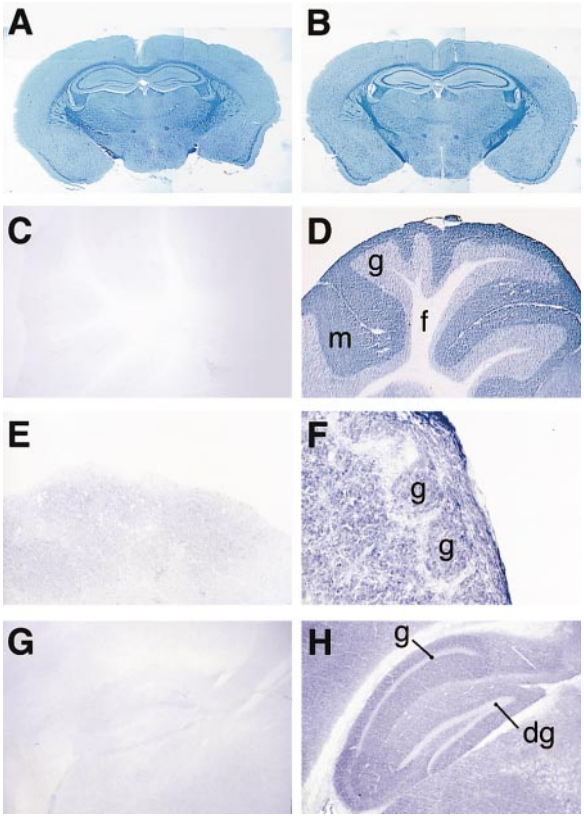

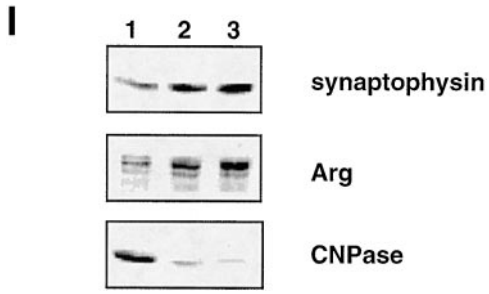

Figure 2. Localization of Arg in Synapse-Rich Regions of the Brain

(A and B) Frontal sections of $arg^{-/-}$ (A) and $arg^{+/+}$ (B) brain stained with Luxol Fast Blue (magnification, 4×).

(C and D) Immunolocalization of Arg in $arg^{-/-}$ (C) and $arg^{+/+}$ (D) cerebellum. Areas immunopositive for Arg stain purple. The molecular layer (m), granular layer (g), and fiber tracts (f) are indicated in (D) (magnification, 10×).

(E and F) Immunolocalization of Arg in $arg^{-/-}$ (E) and $arg^{+/+}$ (F) olfactory bulb glomeruli. The glomeruli are indicated (g) in (F) (magnification, 40×).

(G and H) Immunolocalization of Arg in $arg^{-/-}$ (G) and $arg^{+/+}$ (H) hippocampus. The dentate gyrus (dg) and granular layer (g) are indicated in (H) (magnification, 10ı).

(I) Enrichment of Arg in purified synaptosomes. Western blots containing protein (40 μg) from crude cerebellar lysate (lane 1), the post 1000 g spin supernatant (lane 2), or the purified synaptosome preparation (lane 3) were probed with antibodies to synaptophysin (38 kDa), Arg (135–140 kDa), and CNPase (46 kDa).

Table 2. Behavioral Analysis of $arg^{+/+}$, $arg^{+/-}$, and $arg^{-/-}$ Mice

	$arg^{+/+}$	$arg^{+/-}$	$arg^{-/-}$
(A) Hang test			
Number completed/number tested	9/10	5/7	1/9
(B) Rope climb			
Number completed/number tested	18/20	18/20	6/20
Mean climbing time (min)	2.2 ± 0.4	3.8 ± 0.9	NA
(C) Aggression test			
As residents, mean number of bites delivered (median)	39 ± 12 (42)	24 ± 8 (20)	18 ± 6 (12)
As intruders, mean number of bites received (median)	41 ± 8 (33)	ND	41 ± 7 (41)
(D) Acoustic startle			
Number of responders/number tested	8/9	8/9	2/9
Mean response (V_{avg})	2.0 ± 0.3	2.3 ± 0.4	0.7 ± 0.1
(E) Tactile startle			
Number of responders/number tested	9/9	9/9	9/9
Mean response (V_{avg})	4.4 ± 0.6	5.1 ± 0.6	3.2 ± 0.3
(F) Tail flick			
Time (sec)	0.9 ± 0.1	0.8 ± 0.1	0.9 ± 0.1

Motor skill tests.
(A) Hang Test. The number of mice of each genotype that remained suspended from a wire bar lid for 3 min is presented as a proportion of the number of mice tested.
(B) Rope climbing test. The number of mice that completed the rope climbing test is presented as a proportion of the number of mice tested (top). The mean climbing time (in min ± standard error [SE]) is presented for each genotype (bottom). NA, not applicable (a mean time is not presented because of extensive variability in climbing time for the few $arg^{-/-}$ mice that completed this task).
(C) Aggression test. The mean number of bites (± SE) by resident mice of each genotype as defenders when confronting a naive wild-type intruder mouse (top). The number of bites (± SE) delivered toward mice of each genotype as intruders using a panel of wild-type resident mice (bottom). ND, not determined.
Reflex tests.
(D) Acoustic startle. The number of mice that responded to acoustic startle stimuli is presented as a proportion of the number of mice tested (top). The mean (± SE) response (V_{avg}) of responders of each genotype is presented (bottom).
(E) Tactile Startle. The number of mice that responded to tactile startle stimuli is presented as a proportion of the number of mice tested (top). The mean (± SE) response (V_{avg}) of responders of each genotype is presented (bottom).
(F) Tail flick. The response time of mice to a heat stimulus aimed at the tail is presented. All mice responded in this test. The mean (± SE) response time (in seconds) for each genotype is presented.

the fiber tracts of the cerebellar folia. The glomeruli of the olfactory bulb, where olfactory neurons form synapses with mitral cells and small tufted cells, were also rich in Arg (Figure 2F). However, staining for Arg was very weak in the cell body–rich periglomerular space. Finally, the synapse-rich regions adjacent to the granular layer of the hippocampus showed significant staining for Arg. Again, Arg levels were reduced in the granular layer of the hippocampus that contains mostly cell bodies (Figure 2H). Control immunostaining of $arg^{-/-}$ brains revealed no specific staining (Figures 2C, 2E, and 2G). Despite the high levels of Arg found in the brain, serial sectioning through several $arg^{-/-}$ brains revealed no gross histological abnormalities (Figures 2A and 2B).

Subcellular fractionation experiments revealed that Arg is enriched 2–3-fold in Percoll gradient–purified synaptic terminals (synaptosomes) from cerebellum as compared with crude cerebellar extract (Figure 2I). These synaptosomal preparations were also enriched 2–3-fold in synaptophysin, a protein essential for the secretion of transmitter-containing vesicles at presynaptic termini. Only traces of cyclic nucleotidyl phosphatase (CNPase), a protein abundant in glial cell membranes, were found in the synaptosomal fractions (Figure 2I).

Behavioral Phenotypes in $arg^{-/-}$ Mice

$arg^{-/-}$ mice exhibited multiple behavioral phenotypes (Table 2). At 5 weeks of age, some $arg^{-/-}$ mice placed in an open test field displayed an increased tendency for retropulsion (walking backward) although they were equally active compared with littermate controls. $arg^{-/-}$ mice had difficulty completing tests of motor skill. Only one of nine $arg^{-/-}$ mice tested remained hanging from a wire bar cage lid for the entire test period (3 min), a task accomplished readily by most wild-type (nine of ten) and $arg^{+/-}$ (five of seven) littermate controls, respectively (Table 2A). $arg^{+/+}$ and $arg^{+/-}$ mice easily climbed a 15 cm length of knotted twine, although the mean climbing times for $arg^{+/-}$ mice were longer than for wild-type mice (Table 2B). $arg^{-/-}$ mice rarely (six of twenty) completed the rope climbing test and usually remained hanging on the rope until removed by the investigator. The decrease in motor skills was not simply due to cerebellar dysfunction. $arg^{-/-}$ mice were not ataxic; they did not exhibit an altered gait, and they were able to remain upright when walking on a narrow suspended platform.

Mating and aggression behaviors were also affected by the loss of the *arg* gene. $arg^{-/-}$ mice produced litters

Table 3. Progeny of $abl^{+/-}arg^{+/-}$ Intercrosses

		Embryos (n = 180)		Pups (n = 420)	
arg	*abl*	Expected (%)	Observed (%)	Expected (%)	Observed (%)
+/+	+/+	11 (6.25)	14 (7.8)	26 (6.25)	39 (9.3)
+/+	+/−	23 (12.5)	21 (12)	53 (12.5)	72 (17)
+/+	−/−	11 (6.25)	13 (7.2)	26 (6.25)	13 (3.1)
+/−	+/+	23 (12.5)	18 (10)	53 (12.5)	81 (19)
+/−	+/−	45 (25.0)	46 (26)	105 (25.0)	163 (39)
+/−	−/−	23 (12.5)	16 (8.9)	53 (12.5)	0 (0)
−/−	+/+	11 (6.25)	19 (11)	26 (6.25)	31 (7.4)
−/−	+/−	23 (12.5)	18 (10)	53 (12.5)	21 (5.0)
−/−	−/−	11 (6.25)	15 (8.3)	26 (6.25)	0 (0)

Pups were genotyped between 10 and 14 dpp. Embryos were genotyped at 9.5 dpc. The expected (exp) and observed (obs) frequencies (and percentages) of each genotype are presented. (n = number of progeny analyzed.)

at a reduced frequency as compared with littermate controls, although litter sizes were similar to those of wild-type animals. Male $arg^{-/-}$ mice also displayed less aggression toward intruder mice than did control mice (Table 2C). In a control experiment, $arg^{-/-}$ and $arg^{+/+}$ mice provoked similar levels of attacks when tested as intruders against a panel of wild-type resident mice (Table 2C). Because the overall activity level of the intruder mouse contributes to the number of attacks by residents, this control emphasizes that $arg^{-/-}$ and $arg^{+/+}$ mice are equally active (Miczek and O'Donnell, 1978).

$arg^{-/-}$ mice also showed some abnormal reflexes. Most control $arg^{+/+}$ (eight of nine) and $arg^{+/-}$ (eight of nine) mice were startled by acoustic stimuli (120 dB clicks) (Table 2D). Few $arg^{-/-}$ (two of nine) mice were startled by these stimuli, and the magnitude of the startle responses in the rare $arg^{-/-}$ responder mice was only about 30% of the magnitude of the response of control mice (Table 2D). In contrast, $arg^{-/-}$ mice responded only slightly less well than control mice to tactile (air puff) startle stimuli (Table 2E). $arg^{-/-}$ mice also flicked their tails away from a heat stimulus as quickly as littermate controls (Table 2F).

To identify developmental processes dependent on both Abl and Arg, we intercrossed $abl^{+/-}arg^{+/-}$ animals to create animals with either one or no functional *arg/abl* allele (Table 3).

Phenotypes of Mice with a Single, Functional *arg/abl* Allele

$abl^{-/-}arg^{+/-}$ embryos died between 15.5 and 16.0 dpc. The peritoneum and pericardial sac of many $abl^{-/-}arg^{+/-}$ mice was enlarged and edematous. Most of these animals exhibited recent hemorrhage into the peritoneum or pericardial space (Figure 3).

Only 60% of the expected number of $abl^{+/-}arg^{-/-}$ mice were recovered postnatally. Like $arg^{-/-}$ mice, the surviving $abl^{+/-}arg^{-/-}$ mice were runted at birth and displayed multiple behavioral phenotypes. No gross histological abnormalities were observed in $abl^{+/-}arg^{-/-}$ mice. Unlike the $abl^{-/-}$ mice that exhibit decreased neonatal viability, once born, most $abl^{+/-}arg^{-/-}$ mice survived well into adulthood. In fact, two out of six $abl^{+/-}arg^{-/-}$ females produced litters when mated to wild-type males.

Redundant Roles for Arg and Abl in Neurulation

Neurulation is severely disrupted in $abl^{-/-}arg^{-/-}$ embryos. Delay of neural tube closure is evident in 9.5 dpc $abl^{-/-}arg^{-/-}$ embryos; the rostral third of the neural tube remained open at a time when closure was completed in control littermates (Figures 4A and 4B). At 10.25 dpc, the neural tube of most $abl^{-/-}arg^{-/-}$ embryos had closed, although in some embryos, gaps remained at one or more fusion points in the head region (Figures 4D and 4F).

In contrast to the translucent appearance of the neural tube in control littermates, the neural tube of 10.25 dpc $abl^{-/-}arg^{-/-}$ embryos appeared as a shadowy dark stripe under low-power light microscopy (Figures 4C and 4D). This appearance was due to the collapse of the neuroepithelium of these embryos into the lumen of the neural tube (Figures 5B and 5D). This buckling of the neural tube continues throughout the entire length of the tube (data not shown). The number of mitotic neuroepithelial cells per unit length was similar in 10.25 dpc control and $abl^{-/-}arg^{-/-}$ embryos in the telencephalon, mesencephalon, and rhombencephalon (the presumptive forebrain, midbrain, and hindbrain, respectively) (Figures 5C and 5D; Table 4). The thickness of the neuroepithelium in the mesencephalon and rhombencephalon and the lumenal circumference of the telencephalon and rhombencephalon were also similar in control and $abl^{-/-}arg^{-/-}$ embryos (Table 4). These data show that the defects in $abl^{-/-}arg^{-/-}$ neural tubes were not due to increased thickening or hyperproliferation of the neuroepithelial cells in double mutant embryos.

$abl^{-/-}arg^{-/-}$ embryos from 10.5–11 dpc had massive numbers of apoptotic cells in all tissues of the body (data not shown). The cause of this apoptosis in $abl^{-/-}arg^{-/-}$ embryos was unclear. Blood cells were present in the pericardial sac of one 10.25 dpc $abl^{-/-}arg^{-/-}$ embryo (Figure 5F). Thus, the double mutant embryos, like the $abl^{-/-}arg^{+/-}$ embryos, may have died from hemorrhage.

Defects in the Actin Cytoskeleton of $abl^{-/-}arg^{-/-}$ Neuroepithelial Cells

Consistent with the neurulation defect observed in $abl^{-/-}arg^{-/-}$ embryos, Abl and Arg were expressed in 9–10.25 dpc neuroepithelium (Figures 6 and 7). Abl and Arg were expressed in other tissues at lower levels. In

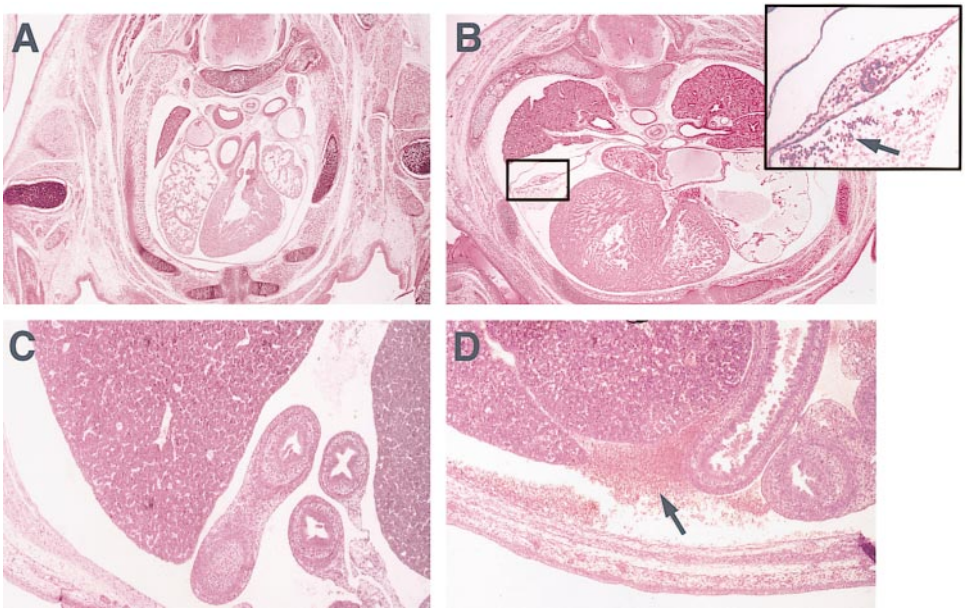

Figure 3. Hemorrhage in 15.5 dpc *abl*$^{-/-}$*arg*$^{+/-}$ Embryos

(A and B) Transverse section of heart from 15.5 dpc *abl*$^{+/-}$*arg*$^{+/-}$ (A) and *abl*$^{-/-}$*arg*$^{+/-}$ (B) embryos stained with H and E. The inset in (B) shows blood cells in pericardium (arrow) (magnification, 5×).

(C and D) Transverse section through peritoneum of 15.5 dpc *abl*$^{+/-}$*arg*$^{+/-}$ (C) and *abl*$^{-/-}$*arg*$^{+/-}$ (D) embryos stained with H and E. Massive numbers of blood cells can be seen in section D (arrow) (magnification, 8×).

9.5 dpc wild-type embryos, actin microfilaments formed a contractile latticework at the lumenal/apical surface of neuroepithelial cells (Figure 7A). The contraction of these filaments contributes to the polarized wedge shape of neuroepithelial cells that is essential for the proper morphogenesis of the neural tube (Karfunkel, 1971; Burnside, 1973). To understand the cellular basis for the malformation of the neural tube in *abl*$^{-/-}$*arg*$^{-/-}$ embryos, we examined the distribution of actin filaments within the columnar cells of the neuroepithelium. In addition to patchy disruptions of the apical actin latticework, disordered ectopic, actin-rich structures were found at the basolateral/marginal surface of the *abl*$^{-/-}$*arg*$^{-/-}$ neuroepithelium (Figure 7B). Interestingly, these abnormal structures were not restricted to the region of the tube where the neuroepithelium had buckled.

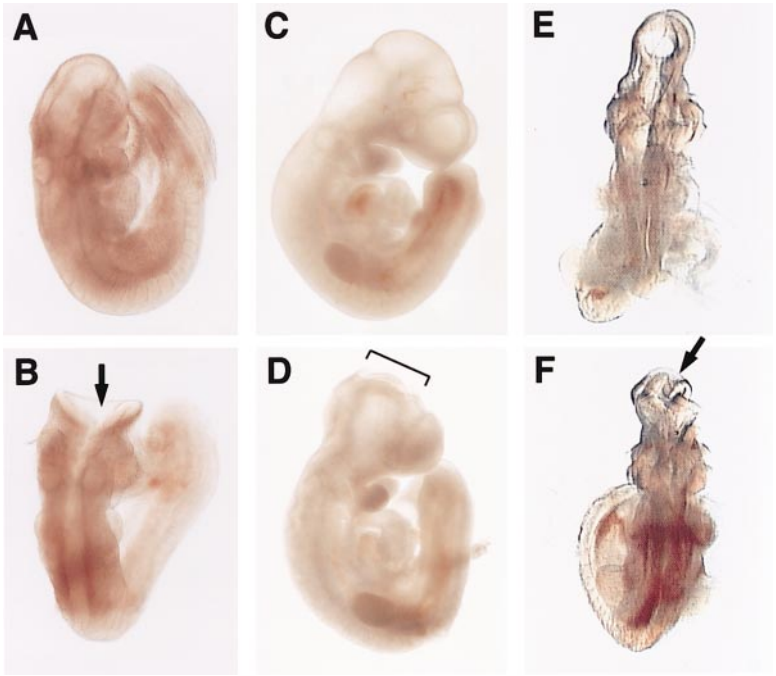

Figure 4. Neural Tube Defects in *abl*$^{-/-}$*arg*$^{-/-}$ Embryos

(A and B) *abl*$^{+/+}$*arg*$^{+/-}$ (A) and *abl*$^{-/-}$*arg*$^{-/-}$ (B) embryos (9.5 dpc) are shown from the dorsal surface. Note that the rostral part of the neural tube remains open in (B) (arrow) (magnification, 20×).

(C and D) *abl*$^{+/+}$*arg*$^{+/-}$ (C) and *abl*$^{-/-}$*arg*$^{-/-}$ (D) embryos (10.25 dpc) are shown from the right side. The *abl*$^{-/-}$*arg*$^{-/-}$ neural tube remains open at only two fusion points in the head (bracket). Note the appearance of the *abl*$^{-/-}$*arg*$^{-/-}$ neural tube as a dark hazy stripe as compared with the translucent appearance of the *abl*$^{+/+}$*arg*$^{+/-}$ neural tube (magnification, 15×).

(E and F) *abl*$^{+/+}$*arg*$^{+/-}$ (E) and *abl*$^{-/-}$*arg*$^{-/-}$ (F) embryos (10.25 dpc) are shown from the dorsal surface. The *abl*$^{-/-}$*arg*$^{-/-}$ neural tube remains open at a fusion point in the head (arrow) (magnification, 15×).

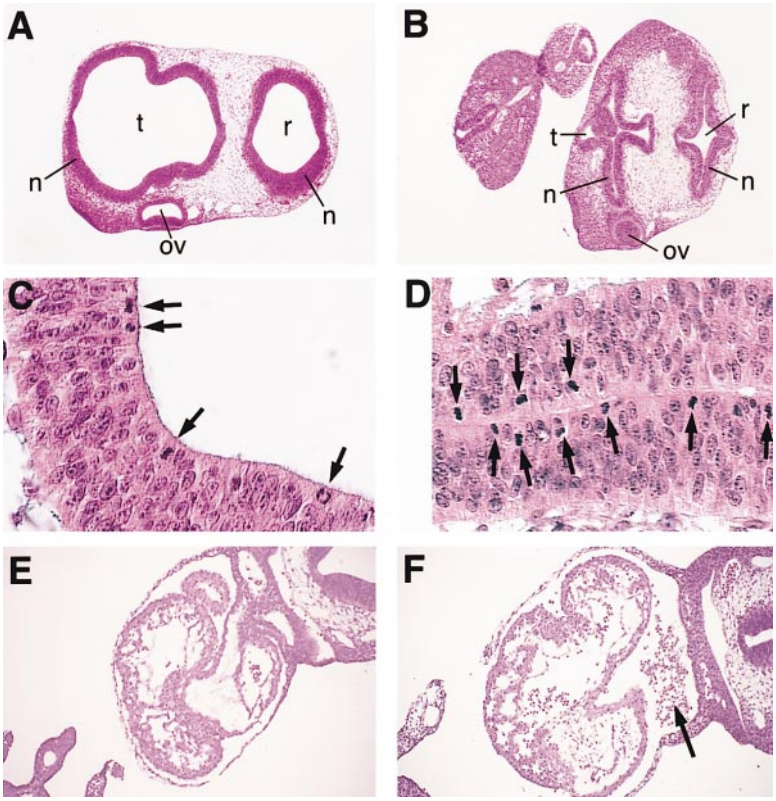

Figure 5. Neurulation Defects and Hemorrhage in $abl^{-/-}arg^{-/-}$ Embryos

(A and B) Transverse sections through the head of 10.5 dpc $arg^{+/-}abl^{+/-}$ (A) and $arg^{-/-}abl^{-/-}$ (B) embryos stained with H and E. The neuroepithelial layer (n) and the lumena of the telencephalon (t) and rhombencephalon (r) are indicated. Both sections are in the plane of the optic vesicle (ov) (magnification, 10×).

(C and D) Transverse sections through the lateral telencephalon of 10.5 dpc $arg^{+/-}abl^{+/-}$ (C) and $arg^{-/-}abl^{-/-}$ (D) embryos stained with H and E. Mitotic figures are indicated (arrows) (magnification, 40×).

(E and F) Transverse sections through the heart of 10.25 dpc $arg^{+/-}abl^{+/-}$ (E) and $arg^{-/-}abl^{-/-}$ (F) embryos stained with H and E. Blood cells are found in the pericardium of the $arg^{-/-}abl^{-/-}$ heart ([F], arrow) (magnification, 15×).

Although we could detect expression of Arg and Abl within the neural tube (Figure 6), the use of thick sections and enzyme-linked detection systems obscured the precise subcellular localization of Abl and Arg in neuroepithelial cells. We localized Abl, Arg, and actin microfilaments in 0.2 μm optical sections using immunofluorescence to better understand how deficiencies in Abl and Arg lead to perturbations of the actin cytoskeleton. A significant portion of both Abl and Arg colocalized at the apical surface of wild-type 10.25 dpc neuroepithelium (Figures 7C–7E). These Abl- and Arg-positive foci were associated with the apical actin latticework (Figure 7E). Abl and Arg also colocalized with actin in several other foci throughout the neural tube. Other regions of the neuroepithelial layer stained selectively for Abl or Arg, albeit at weaker levels than observed in the Abl/Arg/actin-positive foci. This included a portion of Abl that colocalized with nuclear DNA (Figure 7D). In addition, differentiating neurons in the marginal zone showed particularly intense levels of staining for Arg, consistent with the high levels of Arg observed in adult brain (Figures 7C–7E).

Delay in Appearance of MAP2-Positive Early Neurons in $abl^{-/-}arg^{-/-}$ Neuroepithelium

We also evaluated whether the earliest differentiation events that occur within the neural tube were compromised by the loss of Abl and Arg function. The earliest differentiating neurons can be identified by their expression of the neuron-specific MAP2 protein (Huber and

Table 4. Analysis of $abl^{+/-}arg^{+/-}$ and $abl^{-/-}arg^{-/-}$ Neuroepithelium

	Number	Mitoses	Thickness (μm)	Circumference (μm)
Telencephalon				
$abl^{+/-}arg^{+/-}$	5	3.97 ± 1.93	38.7 ± 4.1	876 ± 153
$abl^{-/-}arg^{-/-}$	6	4.63 ± 3.48	26.2 ± 4.1	656 ± 105
Mesencephalon				
$abl^{+/-}arg^{+/-}$	6	3.27 ± 1.08	38.0 ±5.9	ND
$abl^{-/-}arg^{-/-}$	5	3.00 ± 1.78	37.6 ± 11.8	ND
Rhombencephalon				
$abl^{+/-}arg^{+/-}$	5	3.60 ± 0.95	44.7 ± 6.1	474 ± 110
$abl^{-/-}arg^{-/-}$	6	3.95 ± 3.35	39.0 ± 8.9	459 ± 105

$abl^{-/-}arg^{-/-}$ embryos (10.25 dpc) and littermate $abl^{+/-}arg^{+/-}$ controls were sectioned serially and stained with H and E. The number of mitoses per 100 μm of tube length (± SD) and the cross-sectional thickness of the neuroepithelium in μm (± SD) is presented for representative dorsolateral sections taken from the telencephalon, mesencephalon, and rhombencephalon. The total lumenal circumference of the neuroepithelium in μm (± SD) is also presented. The number of embryos used for each set of measurements is shown. ND, not determined.

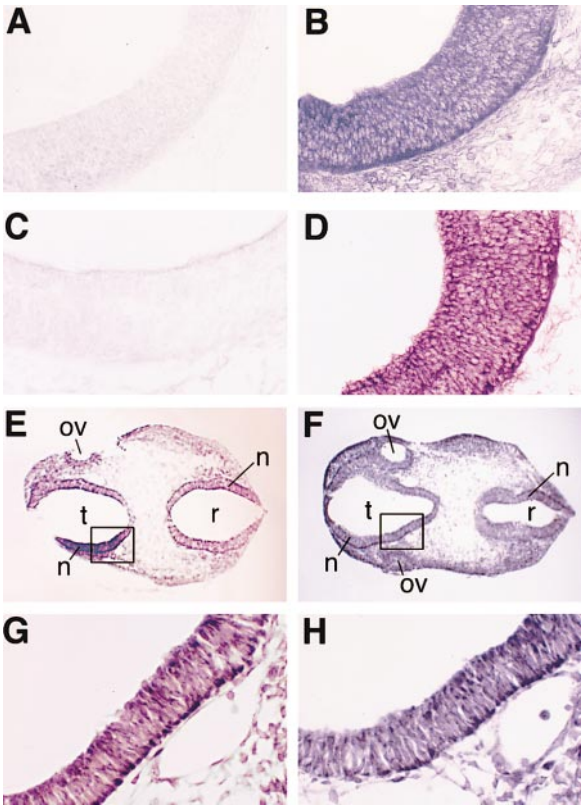

Figure 6. Localization of Arg and Abl within Wild-Type, $arg^{-/-}$, and $abl^{-/-}$ Neuroepithelium

(A and B) Immunolocalization of Arg in 10.25 dpc $arg^{-/-}$ (A) and $arg^{+/+}$ (B) neuroepithelium of the dorsolateral rhombencephalon. Areas immunoreactive for Arg stain purple (magnification, 50×).

(C and D) Immunolocalization of Abl in 10.25 dpc $abl^{-/-}$ (C) and $abl^{+/+}$ (D) neuroepithelium of the dorsolateral rhombencephalon. Areas immunoreactive for Abl stain purple (magnification, 50×).

(E and G) Immunolocalization of Arg in wild-type 9.5 dpc neuroepithelium. Areas immunoreactive for Arg stain purple. The neuroepithelial layer (n) and the lumena of the telencephalon (t) and rhombencephalon (r) are indicated. Area shown boxed in (E) is shown at a higher magnification in (G). Both this section and that shown in (F) are in the plane of the optic vesicles (ov) (magnification, 4× and 40×).

(F and H) Immunolocalization of Abl in wild-type 9.5 dpc neuroepithelium. Areas immunoreactive for Abl stain purple. Area shown boxed in (F) is shown at a higher magnification in (H). Labeling is the same as in (E) (magnification, 4× and 40×).

Matus, 1984). Many MAP2-positive early neurons were identified in the dorsolateral marginal zone of 9.5 dpc $abl^{+/-}arg^{+/-}$ rhombencephalon (Figure 8A). In contrast, few MAP2-positive early neurons could be found in 9.5 dpc $abl^{-/-}arg^{-/-}$ rhombencephalon (Figure 8B). Although the numbers were still reduced relative to control embryos, significantly greater levels of MAP2-positive cells could be found in 10.25 dpc $abl^{-/-}arg^{-/-}$ embryos than in 9.5 dpc $abl^{-/-}arg^{-/-}$ embryos (compare Figures 8B and 8D). Thus, the appearance of MAP2-positive early neurons is delayed in $abl^{-/-}arg^{-/-}$ embryos.

Phosphotyrosine Content in $abl^{-/-}arg^{-/-}$ Embryos

We did not detect any differences in the pattern of the major phosphotyrosine-containing proteins in extracts made from wild-type, $abl^{-/-}$, $arg^{-/-}$, or $abl^{-/-}arg^{-/-}$ 9.5 dpc whole embryos (Figure 1E). The levels of Abl and Arg in these extracts were confirmed by Western blot.

Normal G1/S Checkpoint in $abl^{-/-}arg^{-/-}$ Fibroblasts

The exposure of cycling cells to ionizing radiation arrests cells at the G1/S cell cycle checkpoint and activates Abl kinase activity (Kastan et al., 1992; Kharbanda et al., 1995). We therefore tested the G1/S checkpoint response in two different wild-type or $abl^{-/-}arg^{-/-}$ 3T3 cell lines by measuring the incorporation of bromodeoxyuridine (BrdU) 14 hr after exposure to ionizing radiation (10 Gy). Similar percentages of wild-type and $abl^{-/-}arg^{-/-}$ 3T3 cells arrested in response to ionizing radiation (Figure 8). The growth curves of wild-type and $abl^{-/-}arg^{-/-}$ 3T3 cell lines are also similar (data not shown).

Discussion

Until this work, it was not evident that Abl or Arg played a major role in the cell even though they are widely expressed proteins. $abl^{-/-}$ animals exhibit multiple defects, although these phenotypes appear with variable penetrance (Schwartzberg et al., 1991; Tybulewicz et al., 1991; Hardin et al., 1995). By inactivating the *arg* gene, we have been able to show that the two related proteins must have overlapping functions during development, because an $abl^{-/-}arg^{-/-}$ embryo is much more seriously affected than an animal lacking either gene individually.

It is particularly evident that Abl and Arg play fundamental roles in the development and function of the central nervous system. Arg is very abundant in the adult brain, where it is concentrated in synapses and neuronal processes. $arg^{-/-}$ mice develop normally, and their brains appear normal, but they exhibit multiple behavioral abnormalities. These data suggest that $arg^{-/-}$ brains suffer from defects in neuronal function. However, there are events in neurulation for which either Abl or Arg is necessary. Both proteins colocalize with the apical latticework of actin in the developing neuroepithelium. $abl^{-/-}arg^{-/-}$ embryos exhibit several defects in neurulation. Initially, closure of the neural tube is delayed in $abl^{-/-}arg^{-/-}$ embryos. Then, as the neural tube of $abl^{-/-}arg^{-/-}$ embryos proceeds toward closure, the neuroepithelium buckles into the lumen of the neural tube. These neurulation defects are accompanied by disruptions of the apical network of actin microfilaments and the appearance of ectopic, actin-rich structures at the basolateral surface of $abl^{-/-}arg^{-/-}$ neuroepithelial cells. Finally, the appearance of MAP2-positive early neurons is delayed in $abl^{-/-}arg^{-/-}$ embryos.

Arg Function in the Adult Brain

The localization of Arg to synapses and neuronal processes together with the observed behavioral phenotypes of $arg^{-/-}$ mice suggest that Arg may regulate neurotransmission by phosphorylating proteins at the synapse. The gating properties of several different ion channels are regulated by tyrosine phosphorylation (Holmes et al., 1996; Jayaran et al., 1996; Yu et al., 1997). Similarly, the phosphorylation of an ion channel or other synaptic

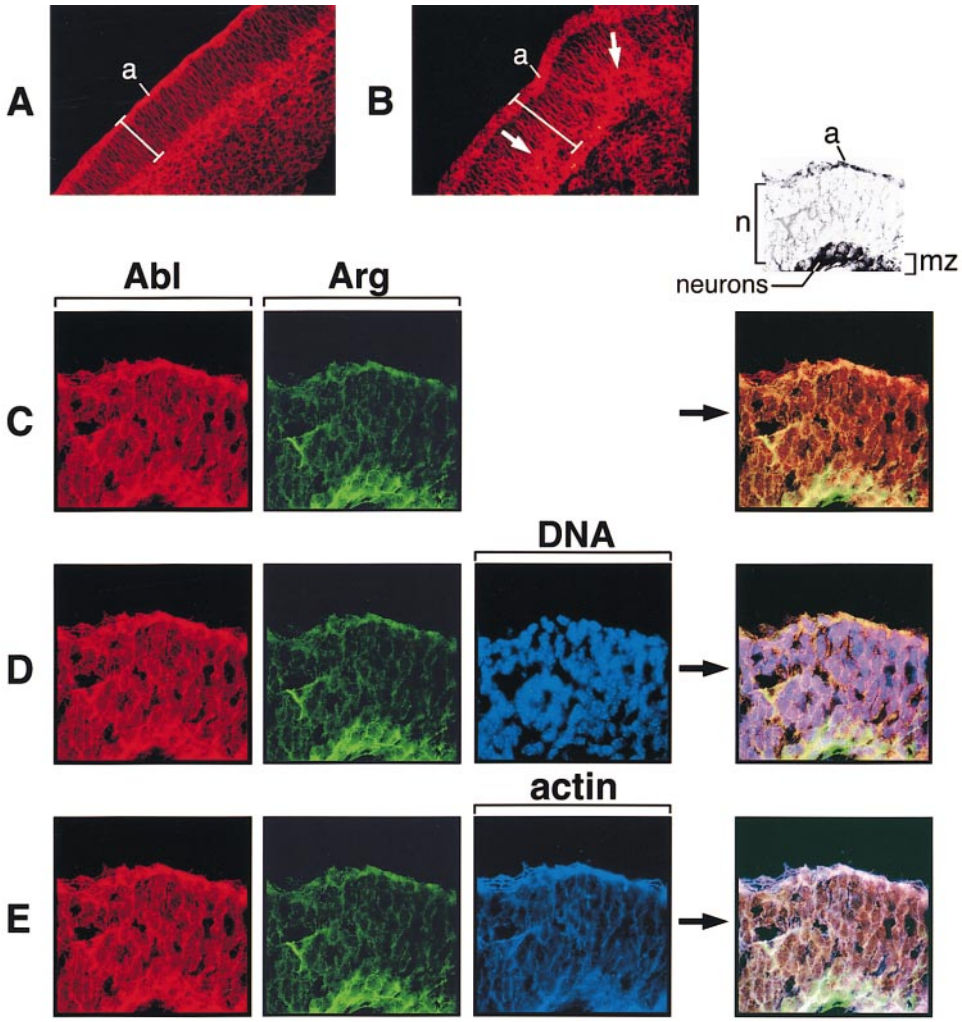

Figure 7. Colocalization of Abl, Arg, and Actin

(A and B) Localization of actin filaments in 9.5 dpc *abl*$^{+/-}$*arg*$^{+/-}$ (A) and *abl*$^{-/-}$*arg*$^{-/-}$ (B) neuroepithelium of the dorsolateral rhombencephalon. Actin filaments were stained with rhodamine-conjugated phalloidin (shown in red). The apical/lumenal surface of the neuroepithelium is to the upper left (a). Brackets indicate the boundary of the neural tube. Ectopic, actin-rich structures are indicated in (B) (arrows).

(Key) (upper right) Black and white drawing depicts a cross-section through 10.25 dpc rhombencephalon used in (C) through (E). The apical surface (a) of the neuroepithelial layer (n) is indicated. The marginal zone (mz) lies below the neuroepithelial layer and contains several differentiating neurons.

(C) Abl (shown in red) and Arg (shown in green) were immunolocalized in a section of 10.25 dpc wild-type neuroepithelium of the dorsolateral rhombencephalon. The merged image shows the area of Abl and Arg colocalization (shown in yellow/orange). Marginal zone early neurons are strongly positive for Arg.

(D) Abl (red), Arg (green), and DNA (blue) were localized as in (C). The merged image shows locations of Abl and Arg colocalization (shown in yellow) and Abl and DNA colocalization (shown in purple).

(E) Abl (red), Arg (green), and actin (blue) were localized as in (C). The merged image shows locations of Abl, Arg, and actin colocalization (shown in white).

protein by Arg may regulate some aspect of neurotransmission. Alternatively, Arg may play a role in intracellular signaling, allowing the neuron to respond appropriately to physical or chemical changes in its environment.

The loss of Arg function probably has differential effects on different types of neurons, because some behaviors and reflexes are more sensitive to the loss of Arg than others. For example, *arg*$^{-/-}$ mice perform normally in the tail flick test, indicating that transmission through the spinal neural circuits is unperturbed by the loss of Arg activity (D'Amour and Smith, 1941). Although they also respond competently to tactile startle stimuli, *arg*$^{-/-}$ mice respond poorly to acoustic startle stimuli. Preliminary experiments have indicated a reduced acoustic brainstem response in *arg*$^{-/-}$ mice, suggesting a sensorineural deficit in these mice (A. J. K. and M. C. Brown, unpublished data).

Abl and Arg in Neurulation: A Role in Actin Dynamics?

The loss of both Abl and Arg function leads to multiple defects in neurulation. Although the regulated division

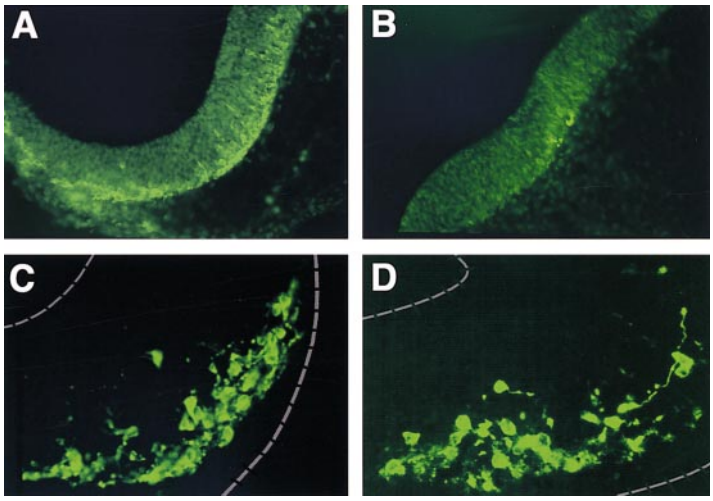

Figure 8. Delay in Appearance of MAP2-Positive Neurons in *abl*$^{-/-}$*arg*$^{-/-}$ Embryos

(A and B) Immunostaining of MAP2-positive cells in 9.5 dpc *abl*$^{+/-}$*arg*$^{+/-}$ (A) and *abl*$^{-/-}$ *arg*$^{-/-}$ (B) dorsolateral rhombencephalon. MAP2-positive early neurons are shown in green. The apical surface is up; the marginal zone is down (magnification, 20×).

(C and D) Immunostaining of MAP2-positive cells in 10.25 dpc *abl*$^{+/-}$*arg*$^{+/-}$ (C) and *abl*$^{-/-}$*arg*$^{-/-}$ (D) dorsolateral rhombencephalon. The apical surface is to the upper left; the marginal zone is down. The borders of the neural tube are indicated in dashed lines (magnification, 40×).

of neuroepithelial cells plays an important role throughout the process of neurulation, we find no evidence for differences in mitotic rate of *abl*$^{-/-}$*arg*$^{-/-}$ neuroepithelial cells as compared with controls (Table 4) (Smith and Schoenwolf, 1997). The neuroepithelial cells of *abl*$^{-/-}$ *arg*$^{-/-}$ embryos do exhibit cytoskeletal alterations. The apical actin latticework is disrupted, and ectopic, actin-rich structures are found at the basolateral surface in *abl*$^{-/-}$*arg*$^{-/-}$ neuroepithelial cells. It is not clear whether alterations in the actin cytoskeleton of the neuroepithelium cause the neurulation defect or whether they are the result of other unknown defects in these embryos. The treatment of salamander embryos with cytochalasin B blocks the apical constriction of neuroepithelial cells and prevents neurulation, thus establishing the importance of actin microfilament dynamics in neurulation (Karfunkel, 1971). Arg and Abl colocalize with the apical actin latticework in neuroepithelial cells, where they may regulate the formation and function of this structure during neurulation. Abl and Arg both have G- and F-actin binding domains through which the kinases might detect or affect changes in the actin cytoskeleton (Van Etten et al., 1994).

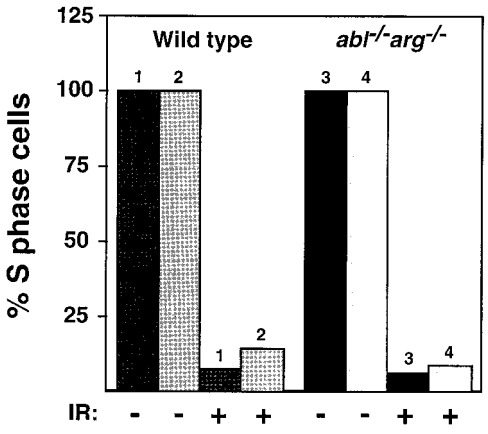

Figure 9. G1/S Checkpoint in *abl*$^{-/-}$*arg*$^{-/-}$ Fibroblasts

Asynchronously growing wild-type (1 and 2) or *abl*$^{-/-}$*arg*$^{-/-}$ (3 and 4) 3T3 cells were mock treated (−IR) or irradiated (+IR) with 10 Gy of γ-irradiation. The percentage of cells in S phase was determined by labeling cells with BrdU for 4 hr beginning 14 hr after irradiation. The percentage of irradiated cells in S phase was normalized to the mock-treated control. Each of the wild-type (1 and 2) and *abl*$^{-/-}$*arg*$^{-/-}$ (3 and 4) 3T3 lines was derived from a separate embryo.

Mena can potentiate the outgrowth of actin-rich structures in cultured fibroblasts (Gertler et al., 1996). A haploinsufficiency in the *enabled* gene of *Drosophila* suppresses the pupal lethality of a *D-abl* mutant fly (Gertler et al., 1990). Thus, too much Enabled is "toxic" in the absence of the D-Abl kinase. Similarly, too much Mena may be toxic in the absence of both Abl family kinases within the developing mouse embryo. During normal development, Arg and Abl may regulate Mena activity to direct the architecture of the actin cytoskeleton. In support of this, one isoform of Mena can be phosphorylated on tyrosine residues, and this Mena isoform is most active in potentiating the formation of actin-rich structures in vivo (Gertler et al., 1996).

Effectors of Abl and Arg Signaling

We found no detectable difference in the pattern of the major phosphotyrosine-containing proteins in tissues and embryos lacking Abl, Arg, or both kinases as compared with wild-type tissues and embryos. More sensitive methods might reveal hypophosphorylated proteins, although they might only be evident after stimulation or other inductive influences. As discussed above, proteins that are tyrosine hypophosphorylated in *arg*$^{-/-}$ synapses may control neuronal shape or function. Proteins that are tyrosine hypophosphorylated in *abl*$^{-/-}$*arg*$^{-/-}$ embryos, but not *abl*$^{-/-}$ or *arg*$^{-/-}$ embryos, might be effectors of the cytoskeletal defects observed in the double mutant neuroepithelial cells.

Although the kinase activity of Abl is essential for rescuing the lethality of *abl*$^{-/-}$ mice (Hardin et al., 1996), mammalian Abl and Arg may have tyrosine kinase–independent functions in vivo. In *Drosophila*, an Abl mutant protein lacking tyrosine kinase activity can rescue the pupal lethality and defective eye development asso-

ciated with *abl* mutations (Henkemeyer et al., 1990). Some of the phenotypes of $arg^{-/-}$ or $abl^{-/-}arg^{-/-}$ mice may similarly reflect a deficiency in this kinase-independent function.

A Role for Abl in the Response to Ionizing Radiation?

Several groups have proposed a role for Abl in the cellular response to genotoxic insult. Some genotoxic stimuli can arrest cells at the G1/S checkpoint and activate Abl kinase activity (Kastan et al., 1992; Kharbanda et al., 1995). Cells that lack the ataxia-telangiectasia mutated or DNA-PK kinases are hypersensitive to ionizing radiation, and Abl is not activated in these cells following treatment with ionizing radiation (Baskaran et al., 1997; Kharbanda et al., 1997; Shafman et al., 1997). However, from previous experiments, it is not clear whether Abl serves as an effector of the G1/S checkpoint. The overexpression of Abl arrests cells in G1, and this cytostatic activity of Abl requires p53 (Sawyers et al., 1994; Goga et al., 1995; Mattioni et al., 1995; Wen et al., 1996). One report indicated that the G1/S checkpoint is compromised in $abl^{-/-}$ mouse embryo fibroblasts (MEFs) (Yuan et al., 1996), whereas another report demonstrated that both G1/S and S phase checkpoints remain intact in $abl^{-/-}$ MEFs (Liu et al., 1996). We find that the G1/S checkpoint is intact in $abl^{-/-}arg^{-/-}$ 3T3 cell lines. It is doubtful, therefore, that Abl or Arg is a crucial effector of the G1/S checkpoint.

Functional Redundancy between Abl and Arg in Other Tissues

It is not clear how reductions of Arg gene dosage in an $abl^{-/-}$ background lead to the hemorrhage observed in $abl^{-/-}arg^{+/-}$ and $abl^{-/-}arg^{-/-}$ embryos. The observation that Abl kinase activity can be activated by the attachment of cells to fibronectin suggests that Abl and Arg may both mediate signals derived from cell–cell or cell–substrate adhesion (Lewis et al., 1996). In the absence of Abl, reductions in Arg copy number may lead to dosage-sensitive alterations in cellular shape or adhesiveness. Such alterations in endothelial cells or platelets could contribute to the hemorrhage observed in $abl^{-/-}arg^{+/-}$ and $abl^{-/-}arg^{-/-}$ embryos.

The experiments presented here reveal that Abl and Arg both play essential roles during neurulation. These observations suggest that Abl and Arg may target similar substrates in vivo. In tissue culture cells, Abl has been found in both the nucleus and the cytoplasm, whereas Arg is cytoplasmic (Van Etten et al., 1989; Lewis et al., 1996; Wang and Kruh, 1996). Simultaneous staining for Abl, Arg, and nuclear DNA revealed that Abl and Arg colocalize in the cytoplasm of neuroepithelial cells (Figure 7C). Therefore, the redundant functions performed by these kinases in the neuroepithelium probably occur in the cytoplasm. Studying cells from mutant embryos, we have not seen growth or checkpoint defects, raising the question of what important nuclear function Abl might play. It seems likely that as a part of its activity, Abl carries information about the cytoplasm into the nucleus, but how it integrates that information into cellular behavior remains obscure.

Finally, several studies have revealed that multiple Src family tyrosine kinases also overlap functionally in a wide variety of tissues and cell types (Lowell and Soriano, 1996). Because of their wide distribution and conservation of structure, it is likely that Abl and Arg play functionally redundant roles in cellular and developmental processes that have yet to be studied.

Experimental Procedures

Construction of the *arg* Targeting Construct

Multiple mouse *arg* cDNAs were isolated from mouse thymus and brain UNI-ZAP XR libraries (Stratagene, La Jolla, CA) with a DNA probe encoding the SH3-SH2 kinase domain of human Arg (a kind gift of Gary Kruh). Genomic clones containing the *arg* coding sequence were cloned from 129/SvJ mouse liver genomic library and mapped and sequenced by using 25 bp oligodeoxynucleotides corresponding to the sequence of mouse *arg* cDNA.

To construct the *arg* targeting vector, a 4.2 kb Xba-SacI piece of *arg* genomic DNA was placed into the XhoI site of pPNT plasmid (Tybulewicz et al., 1991) in opposite transcriptional orientation to the PGK-neo^R cassette to create pTK205.11. The 5 kb KpnI-EcoRV piece of *arg* genomic DNA was inserted into the XbaI-KpnI sites of pTK205.11 to create the *arg* targeting vector pTK206.6. This vector was electroporated into J1 ES cells. Clones were selected in G418 and Ganciclovir. BglII-digested genomic DNA was probed with a 1.8 kb BglII-KpnI probe upstream of the 5′ end of the construct to detect correctly targeted ES cells. Homologous recombinants were identified in 8 of 223 clones. $arg^{+/-}$ and $arg^{-/-}$ mice were generated as described (Li et al., 1992).

Antibody Generation, Western Blotting, and Immunohistochemistry

Antibodies to GST–Arg fusion proteins were raised in rabbits. GST–Arg fusion proteins were made by PCR amplification of Arg residues 112–259, 558–658, and 962–1152 and insertion into pGEX2T.

Tissue samples were disrupted in radio immunoprecipitation assay buffer containing protease inhibitors on ice, and the protein was determined by the Bio-Rad assay (Mellville, NY). Each extract (100 μg) was separated on a 7.5% SDS-PAGE gel. The gel was blotted to Immobilon P membrane and probed with antibodies specific to Arg (residues 558–658), Abl (Pharmingen, San Diego, CA), and phosphotyrosine (Upstate Biotechnology, Lake Placid, NY), followed by secondary antibodies coupled to horseradish peroxidase. The blots were developed by chemiluminescent detection.

Control and $arg^{-/-}$ brains were removed, flash frozen in O. C. T. resin (Sakura FineTek, Torrance, CA), and cut into 10 μm sections on a cryostat. The sections were fixed in ice-cold fresh 2% paraformaldehyde in PBS for 10 min, permeabilized for 5 min in PBS + 0.1% Triton X-100, blocked in PBST + G (PBS + 0.05% Tween 20 + 5% normal goat serum) for 30 min, incubated with anti-Arg antibodies at 200 ng/ml in PBST + G for 1 hr, washed 3 × 5 min in PBST, incubated with biotinylated goat anti-rabbit IgG (Jackson Immunoresearch, West Grove, PA) (1:1000 dilution) for 1 hr, washed 3 × 5 min in PBST, and developed by the ABC-Alkaline phosphatase or ABC-Horseradish peroxidase systems (Vector Laboratories, Burlingame, CA).

Embryos were obtained from timed matings of $abl^{+/-}arg^{+/-}$ males to $abl^{+/-}arg^{+/-}$ females and fixed in ice-cold 2% paraformaldehyde in PBS (30 min for 9.5 dpc, 45 min for 10–11.5 dpc). Following fixation, embryos were rinsed several times in PBS, cryoprotected in PBS/15% sucrose, and frozen in O. C. T. Sections (14 μm) were cut and stained as above for Arg. Sections were stained for Abl as previously described with the ABC-Alkaline phosphatase for detection (Lewis et al., 1996). For immunofluorescence, actin was localized with rhodamine or Oregon Green conjugated–phalloidin (Molecular Probes, Eugene, OR). After incubation with primary antibodies, Abl and Arg were detected with anti-mouse Texas Red or anti-rabbit

Cy5 secondary antibodies (Jackson Immunoresearch, West Grove, PA). MAP2-positive cells were identified with a monoclonal antibody to MAP2 (Sigma, St. Louis, MO), followed by an FITC-labeled secondary antibody. DNA was stained with DAPI at 1 μg/ml. Images were captured on a Deltavision Optical Section Deconvolution Microscope (Applied Precision, Issaquah, WA).

Histology

Embryos were fixed in Bouin's fixative, embedded in paraffin, sectioned (8 μm sections), and stained with hematoxylin and eosin (H and E). Two transverse sections from the dorsolateral portions of the telencephalon (level of optic vesicle), mesencephalon (mid-region), and rhombencephalon (mid-region) of each embryo were photographed at 40× magnification. The number of mitotic figures per unit length of neuroepithelium and the thickness of the neuroepithelial layer were measured from these sections. The total lumenal circumference of transverse sections was measured from photographs taken at 4×. Adult mice were fixed by perfusion with Bouin's fixative. Alternating serial sections were stained with H and E or Luxol Fast Blue.

FACS Analysis

Fluorescence-activated cell sorter (FACS) analysis of spleen, thymus, bone marrow, and blood cells was performed essentially as described (Horwitz et al., 1997) with commercially available antibodies that recognize B and T lymphocytes, granulocytes, macrophages, and erythroblasts.

Purification of Synaptosomes

Synaptosomes were purified as published (Meffert et al., 1994). Monoclonal antibodies to synaptophysin (Sigma, St. Louis, MO) and CNPase (Accurate Scientific, Westbury, NY) were used at a 1:500 dilution. The enrichment of Arg and synaptophysin was estimated by comparing the signals of a 1:1 dilution series of crude extract and purified synaptosomes on the same Western Blot.

Behavioral Analysis

Behavioral tests were conducted by using standard guidelines as outlined below. For each test, mice from at least five different litters were used.

Open Field Test

Mice were placed in a 1 × 1 m square open test field surrounded by an 8 cm high opaque wall (Goldowitz et al., 1992). Each mouse was videotaped for 10 min, and data were collected by a digital tracking device. $arg^{-/-}$ mice did not differ from littermate controls in total distance traveled.

Hang Test

Mice were placed on top of a wire bar cage lid (Goldowitz et al., 1992). The screen was inverted slowly, and the ability to remain suspended for 3 min was noted for each mouse.

Rope Climbing Test

Mice were placed at the bottom of a 15 cm length of twine (0.3 cm thick with knots at 1.5 cm intervals) suspended from a 2 × 5 cm platform (Goldowitz et al., 1992). The time that each mouse required to climb the rope was noted. Mice that failed to complete the task by the end of 20 min were removed from the rope.

Aggression Test

Ten-week-old male mice were housed in mating pairs (Miczek and O'Donnell, 1978). Ten minutes prior to testing, the female and pups were removed. A 10-week-old male Swiss Webster intruder was placed in the cage. After the initial attack, the cage was videotaped for 5 min. The number of bites administered by the resident on the intruder was counted upon review of the videotape.

Startle Test

Ten-week-old male mice were placed in a restraint attached to a displacement meter (Paylor and Crawley, 1977). After 5 min of acclimatization, the mice were exposed to 20 air puffs (20 psi delivered by an air nozzle placed above the spine) or 20 clicks (of 120 dB) delivered randomly over a period of 10 min. The V_{max} and V_{avg} of the displacement meter were recorded automatically.

Tail Flick

The Tail Flick Apparatus contains a photosensor located directly beneath a focused red light beam (D'Amour and Smith, 1941). The tails of 10-week-old male mice were placed in a groove between the light and the photosensor. Following activation of the light, the time required to activate the photosensor was recorded automatically. The median response time for each mouse was used to compute the mean response time for each genotype.

Analysis of G1/S Checkpoint

Embryonic fibroblasts made from 9.5 dpc embryos were passaged every 3 days at 1×10^6 cells per 10 cm plate in Dulbecco's Modified Eagle Medium containing 15% fetal calf serum until immortalized. Dependent on the cell batch, this required between 20 and 30 passages. G1/S checkpoint analysis was performed as described (Xu and Baltimore, 1996).

Acknowledgments

We would like to thank S. Boast and S. Goff (Columbia University) for advice and the gift of *abl*^{2} mice (Tybulewicz et al., 1991) and F. Gertler (Massachussetts Institute of Technology), who first noted a significant portion of Abl in the cytoplasm of mouse tissue sections, for assistance in analyzing images. We would like to thank the members of the Gertler, Miczek, and Baltimore Labs for helpful discussions during the course of this work. We are also grateful for the helpful suggestions of two anonymous reviewers. A. J. K. would like to thank M. C. Brown, F. Gertler, B. Howell, T. Jacks, A. McClatchey, G. Schneider, P. Soriano, and especially C. Lois for helpful discussions. This work was supported by a Fellowship from the Jane Coffin Childs Memorial Fund for Cancer Research (A. J. K.), a Special Fellowship from the Leukemia Society of America (A. J. K.), and United States Public Health Service research grants AA5122 and DA02632 (K. A. M.) and CA51462 (D. B.).

Received July 23, 1998; revised November 10, 1998.

References

Baskaran, R., Wood, L.D., Whitaker, L.L., Canman, C.E., Morgan, S.E., Xu, Y., Barlow, C., Baltimore, D., Wynshaw-Boris, A., Kastan, M.B., and Wang, J.Y.J. (1997). Ataxia telangiectasia mutant protein activates c-Abl tyrosine kinase in response to ionizing radiation. Nature *387*, 516–519.

Burnside, B. (1973). Microtubules and microfilaments in amphibian neurulation. Am. J. Zool. *13*, 989–1006.

Dai, Z., and Pendergast, A.M. (1995). Abi-2, a novel SH3-containing protein interacts with the c-Abl tyrosine kinase and modulates c-Abl transforming activity. Genes Dev. *9*, 2569–2582.

Daley, G.Q., and Ben-Neriah, Y. (1991). Implicating the Bcr-Abl gene on the pathogenesis of Philadephia chromosome positive human leukemia. Adv. Cancer Res. *57*, 151–184.

D'Amour, F.E., and Smith, D.L. (1941). A method for determining loss of pain sensation. J. Pharmacol. Exp. Ther. *72*, 74–79.

Gertler, F.B., Bennett, R.L., Clark, M.J., and Hoffmann, F.M. (1989). Drosophila abl tyrosine kinase in embryonic CNS axons: a role in axonogenesis is revealed through dosage-sensitive interactions with disabled. Cell *58*, 103–113.

Gertler, F.B., Doctor, J.S., and Hoffmann, F.M. (1990). Genetic suppression of mutations in the *Drosophila* abl proto-oncogene homolog. Science *248*, 857–860.

Gertler, F.B., Hill, K.K., Clark, M.J., and Hoffmann, F.M. (1993). Dosage-sensitive modifiers of *Drosophila* abl tyrosine kinase function: prospero, a regulator of axonal outgrowth, and disabled, a novel tyrosine kinase substrate. Genes Dev. *7*, 441–453.

Gertler, F.B., Niebuhr, K., Reinhard, M., Wehland, J., and Soriano, P. (1996). Mena, a relative of VASP and Drosophila enabled is implicated in the control of microfilament dynamics. Cell *87*, 227–239.

Goga, A., Liu, X., Hambuch, T.M., Senechal, K., Major, E., Berk, A.J., Witte, O.N., and Sawyers, C.L. (1995). P53-dependent growth suppression by the c-Abl nuclear tyrosine kinase. Oncogene *11*, 791–799.

Goldowitz, D., Wahlsten, D., and Wimer, R.E., eds. (1992). Techniques for the Genetic analysis of Brain and Behavior: Focus on the Mouse (New York: Elsevier Press).

Golub, T.R., Goga, A., Barker, G.F., Afar, D.E., McLaughlin, J., Bohlander, S.K., Rowley, J.D., Witte, O.N., and Gilliland, D.G. (1996). Oligomerization of the ABL tyrosine kinase by the Ets protein TEL in human leukemia. Mol. Cell. Biol. *16*, 4107–4116.

Hardin, J.D., Boast, S., Schwartzberg, P.L., Lee, G., Alt, F.W., Stall, A.M., and Goff, S.P. (1995). Bone marrow B lymphocyte development in c-abl-deficient mice. Cell. Immunol. *165*, 44–54.

Hardin, J.D., Boast, S., Mendelsohn, M., de los Santos, K., and Goff, S.P. (1996). Transgenes encoding both type I and type IV c-abl proteins rescue the lethality of c-abl mutant mice. Oncogene *12*, 2669–2677.

Henkemeyer, M., West, S.R., Gertler, F.B., and Hoffmann, F.M. (1990). A novel tyrosine kinase-independent function of Drosophila *abl* correlates with proper subcellular localization. Cell *63*, 949–960.

Holmes, T.C., Fadool, D.A., Ren, R., and Levitan, I.B. (1996). Association of Src tyrosine kinase with a human potassium channel mediated by SH3 domain. Science *274*, 2089–2091.

Horwitz, B.H., Scott, M.L., Cherry, S.R., Bronson, R.T., and Baltimore, D. (1997). Failure of lymphopoiesis after adoptive transfer of NF-kB-deficient fetal liver cells. Immunity *6*, 765–772.

Huber, G., and Matus, A. (1984). Differences in the cellular distributions of two microtubule-associated proteins, MAP1 and MAP2, in the brain. J. Neurosci. *4*, 151–160.

Jayaran, T., Ondrias, K., Ondriasova, E., and Marks, A.R. (1996). Regulation of the inositol 1,4,5-trisphosphate receptor by tyrosine phosphorylation. Science *272*, 1492–1494.

Karfunkel, P. (1971). The activity of microtubules and microfilaments in neurulation in the chick. J. Exp. Zool. *181*, 289–302.

Kastan, M.B., Zhan, Q., El-Deiry, W.S., Carrier, F., Jacks, T., Walsh, W.V., Plunkett, B.S., Vogelstein, B., and Fornace, J.A.J. (1992). A mammalian cell cycle checkpoint pathway utilizing p53 and *GADD45* is defective in ataxia-telangiectasia. Cell *71*, 587–597.

Kharbanda, S., Ren, R., Pandey, P., Shafman, T.D., Feller, S.M., Weichselbaum, R.R., and Kufe, D.W. (1995). Activation of the c-Abl tyrosine kinase in the stress response to DNA-damaging agents. Nature *376*, 785–788.

Kharbanda, S., Pandey, P., Jin, S., Inoue, S., Bharti, A., Yuan, Z.-M., Weichselbaum, R., Weaver, D., and Kufe, D. (1997). Functional interaction between DNA-PK and c-Abl in response to DNA damage. Nature *386*, 732–735.

Kruh, G.D., King, C.R., Kraus, M.H., Popescu, N.C., Amsbaugh, S.C., McBride, W.O., and Aaronson, S.A. (1986). A novel human gene closely related to the abl proto-oncogene. Science *234*, 1545–1548.

Lewis, J.M., Baskaran, R., Taagepera, S., Schwartz, M.A., and Wang, J.Y.J. (1996). Integrin regulation of c-Abl tyrosine kinase activity and cytoplasmic-nuclear transport. Proc. Natl. Acad. Sci. USA *93*, 15174–15179.

Li, E., Bestor, T.H., and Jaenisch, R. (1992). Targeted mutation of the DNA methyltransferase gene results in embryonic lethality. Cell *69*, 915–926.

Liu, Z.-G., Baskaran, R., Lea-Chou, E.T., Wood, L.D., Chen, Y., Karin, M., and Wang, J.Y.J. (1996). Three distinct signaling responses by murine fibroblasts to genotoxic stress. Nature *384*, 273–276.

Lowell, C.A., and Soriano, P. (1996). Knockouts of Src-family kinases: stiff bones, wimpy T cells, and bad memories. Genes Dev. *10*, 1845–1857.

Mattioni, T., Jackson, P.K., van Huijsduijnen, O.B.-H., and Picard, D. (1995). Cell cycle arrest by tyrosine kinase Abl involves altered early mitogenic response. Oncogene *10*, 1325–1333.

Mayer, B.J., and Baltimore, D. (1994). Mutagenic analysis of the roles of SH2 and SH3 domains in regulation of the Abl tyrosine kinase. Mol. Cell. Biol. *14*, 2883–2894.

McWhirter, J.R., and Wang, J.Y. (1991). Activation of tyrosine kinase and microfilament-binding functions of c-abl by bcr sequences in bcr/abl fusion proteins. Mol. Cell. Biol. *11*, 1553–1565.

Meffert, M.K., Premack, B.A., and Schulman, H. (1994). Nitric oxide stimulates Ca^{2+}-independent synaptic vesicle release. Neuron *12*, 1235–1244.

Miczek, K.A., and O'Donnell, J.M. (1978). Intruder-evoked aggression in isolated and nonisolated mice: effects of psychomotor stimulants and 1-dopa. Psychopharmacology *57*, 47–55.

Mysliwiec, T., Perego, R., and Kruh, G.D. (1996). Analysis of chimeric Gag-Arg/Abl molecules indicates a distinct negative regulatory role for the Arg C-terminal domain. Oncogene *12*, 631–640.

Paylor, R., and Crawley, J.N. (1977). Inbred strain differences in prepulse inhibition of the mouse startle response. Psychopharmacology *132*, 169–180.

Ren, R., Ye, Z.S., and Baltimore, D. (1994). Abl protein-tyrosine kinase selects the Crk adapter as a substrate using SH3-binding sites. Genes Dev. *8*, 783–795.

Rosenberg, N., and Witte, O.N. (1988). The viral and cellular forms of the Abelson (abl) oncogene. Adv. Virus Res. *35*, 39–81.

Salgia, R., Li, J.L., Ewaniuk, D.S., Pear, W., Pisick, E., Burky, S.A., Ernst, T., Sattler, M., Chen, L.B., and Griffin, J.D. (1997). BCR/ABL induces multiple abnormalities of cytoskeletal function. J. Clin. Invest. *100*, 46–57.

Sawyers, C.L., McLaughlin, J., Goga, A., Havlik, M., and Witte, O. (1994). The nuclear tyrosine kinase c-Abl negatively regulates cell growth. Cell *77*, 121–131.

Shafman, T., Khanna, K.K., Kedar, P., Spring, K., Kozlov, S., Yen, T., Hobson, K., Gatei, N., Zhang, N., Watters, D., Egerton, M., et al. (1997). Interaction between ATM protein and c-Abl in response to DNA damage. Nature *387*, 520–523.

Schwartzberg, P.L., Stall, A.M., Hardin, J.D., Bowdish, K.S., Humaran, T., Boast, S., Harbison, M.L., Robertson, E.J., and Goff, S.P. (1991). Mice homozygous for the ablm1 mutation show poor viability and depletion of selected B and T cell populations. Cell *65*, 1165–1175.

Shi, Y., Alin, K., and Goff, S. (1995). Abl-interactor-1, a novel SH3 protein binding to the C-terminal portion of the Abl protein, suppresses v-abl transforming activity. Genes Dev. *9*, 2583–2597.

Smith, J.L., and Schoenwolf, G.C. (1997). Neurulation: coming to closure. Trends Neurosci. *20*, 510–517.

Tybulewicz, V.L., Crawford, C.E., Jackson, P.K., Bronson, R.T., and Mulligan, R.C. (1991). Neonatal lethality and lymphopenia in mice with a homozygous disruption of the c-abl proto-oncogene. Cell *65*, 1153–1163.

Van Etten, R.A., Jackson, P., and Baltimore, D. (1989). The mouse type IV c-abl gene product is a nuclear protein, and activation of transforming ability is associated with cytoplasmic localization. Cell *58*, 669–678.

Van Etten, R.A., Jackson, P.K., Baltimore, D., Sanders, M.C., Matsudaira, P.T., and Janmey, P.A. (1994). The COOH terminus of the c-Abl tyrosine kinase contains distinct f- and g-actin binding domains with bundling activity. J. Cell Biol. *124*, 325–340.

Wang, B., and Kruh, G.D. (1996). Subcellular localization of the Arg protein tyrosine kinase. Oncogene *13*, 193–197.

Wang, B., Mysliwiec, T., Krainc, D., Jensen, R.A., Sonoda, G., Testa, J.R., Golemis, E.A., and Kruh, G.D. (1996). Identification of ArgBP1, an Arg protein tyrosine kinase binding protein that is the human homologue of a CNS-specific *Xenopus* gene. Oncogene *12*, 1921–1929.

Wang, J.Y., Ledley, F., Goff, S., Lee, R., Groner, Y., and Baltimore, D. (1984). The mouse c-abl locus: molecular cloning and characterization. Cell *36*, 349–356.

Wen, S.-T., Jackson, P.K., and Van Etten, R.A. (1996). The cytostatic function of c-Abl is controlled by multiple nuclear localization signals and requires the *p53* and *Rb* tumor suppressor gene products. EMBO J. *15*, 1583–1595.

Xu, Y., and Baltimore, D. (1996). Dual roles of ATM in the cellular response to radiation and in cell growth control. Genes Dev. *10*, 2401–2410.

Yu, X.-M., Askalan, R., Keill, G.J., II, and Salter, M.W. (1997). NMDA channel regulation by channel-associated protein tyrosine kinase Src. Science *275*, 674–678.

Yuan, X.-M., Huang, Y., Whang, Y., Sawyers, C., Weichselbaum, R., Kharbanda, S., and Kufe, D. (1996). Role for c-Abl tyrosine kinase in growth arrest response to DNA damage. Nature *382*, 272–274.